Electronic Supplementary Information for:

Optimizing plasmon enhanced luminescence in silicon nanocrystals by gold nanorods

Ondřej Pavelka[a], Sergey Dyakov[b], Jozef Veselý[c], Anna Fučíková[a], Hiroshi Sugimoto[d], Minoru Fujii[d], Jan Valenta[a]

[a] Department of Chemical Physics and Optics, Faculty of Mathematics and Physics, Charles University, Ke Karlovu 3, 121 16, Prague, Czech Republic

[b] Photonics & Quantum Materials Center, Skolkovo Institute of Science and Technology, Nobel Street 3, Moscow 143025, Russia

[c] Department of Physics of Materials, Faculty of Mathematics and Physics, Charles University, Ke Karlovu 3, 121 16, Prague, Czech Republic

[d] Department of Electrical and Electronic Engineering, Graduate School of Engineering, Kobe University, Rokkodai, Nada, Kobe 657-8501, Japan

1. Size distributions of AuNRs

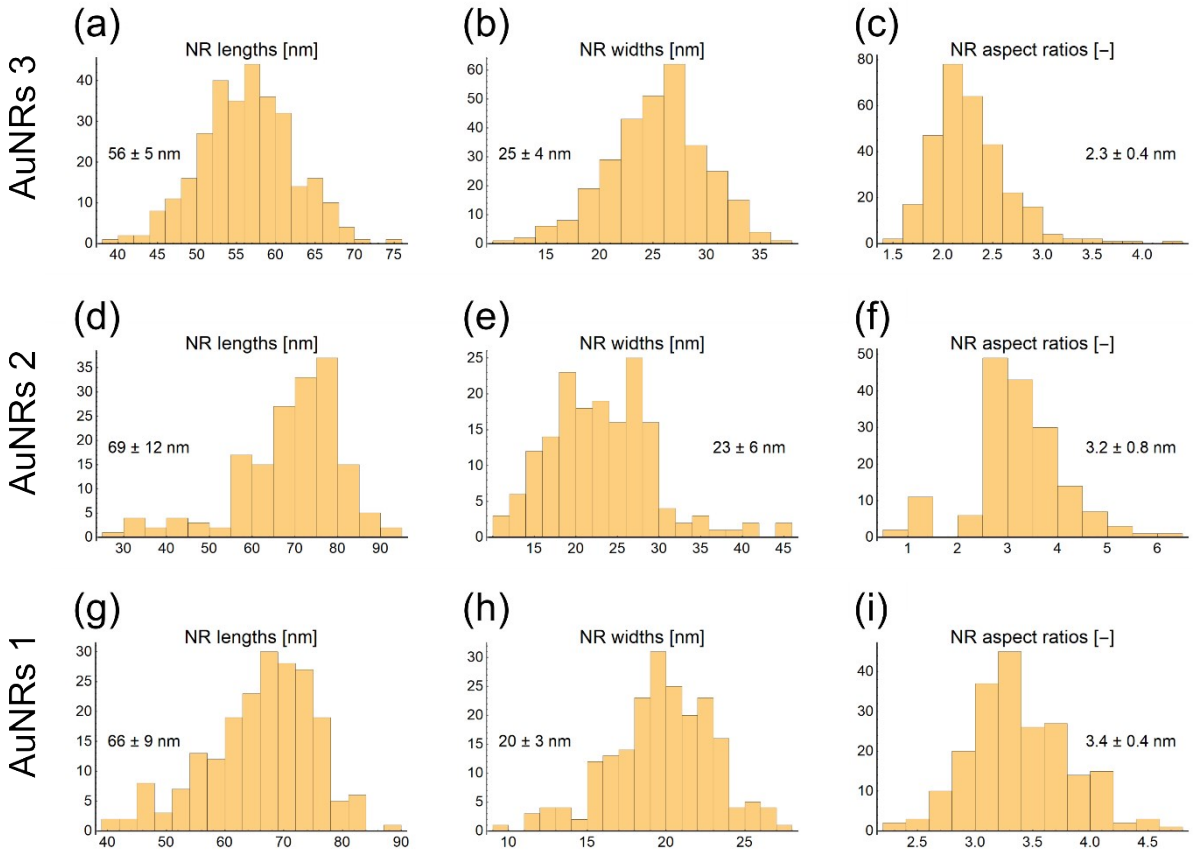

Figure S1: Size distributions of AuNRs used in the experiments with SiNCs. For each sample the distribution and the corresponding mean value of nanorod lengths, widths and aspect ratios is shown. (a, b, c) AuNRs 3, (d, e, f) AuNRs 2, (g, h, i) AuNRs 3.

2. Complementary EFTEM images

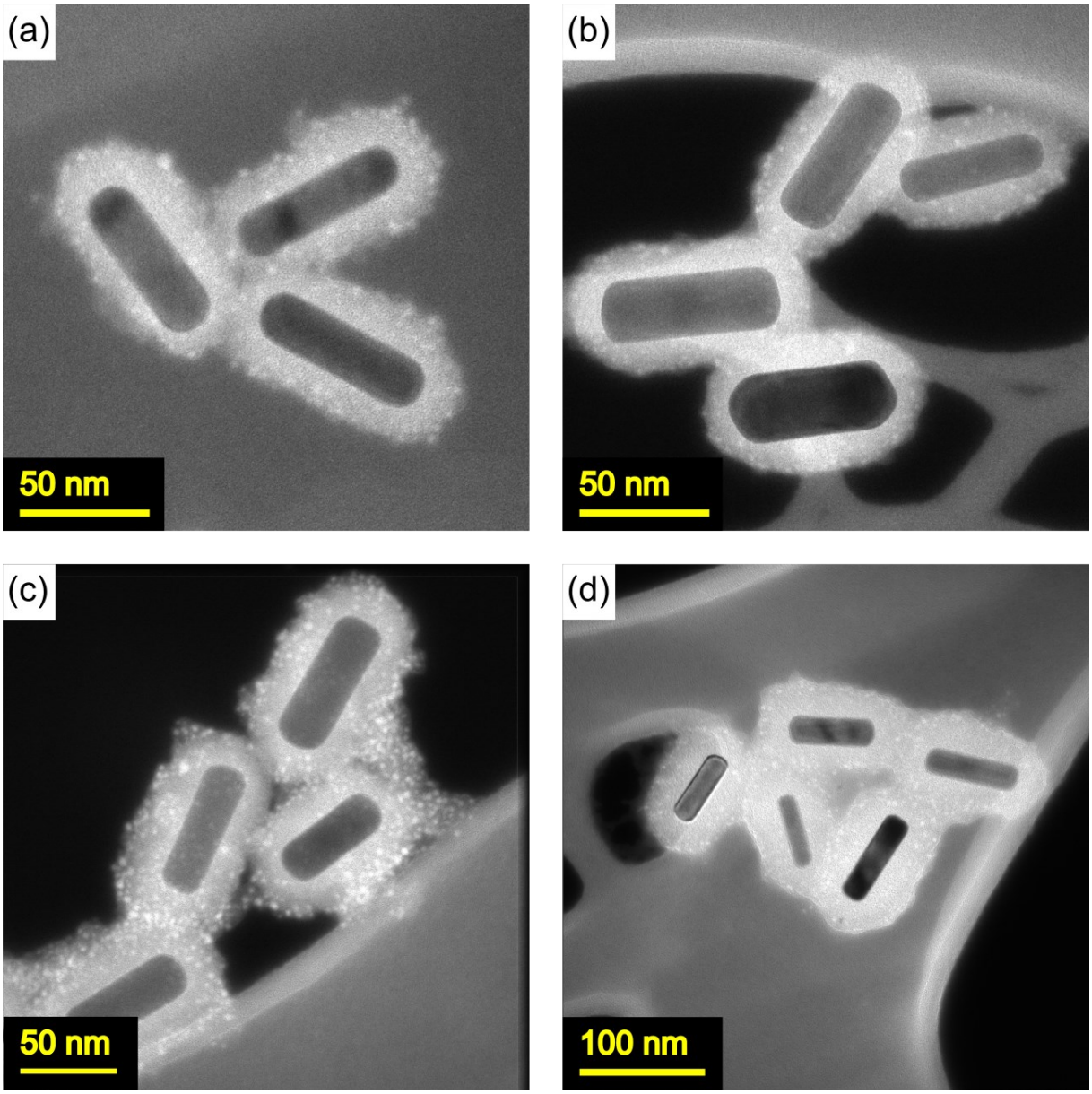

Figure S2: EFTEM images of SiNCs attached to Au@SiO2NRs with varying SiO2 shell thicknesses. (a) AuNRs 1 with 11 nm shell, (b) AuNRs 2 with 13 nm shell, (c) AuNRs 2 with 17 nm shell, (d) AuNRs 1 with 21 nm shell.

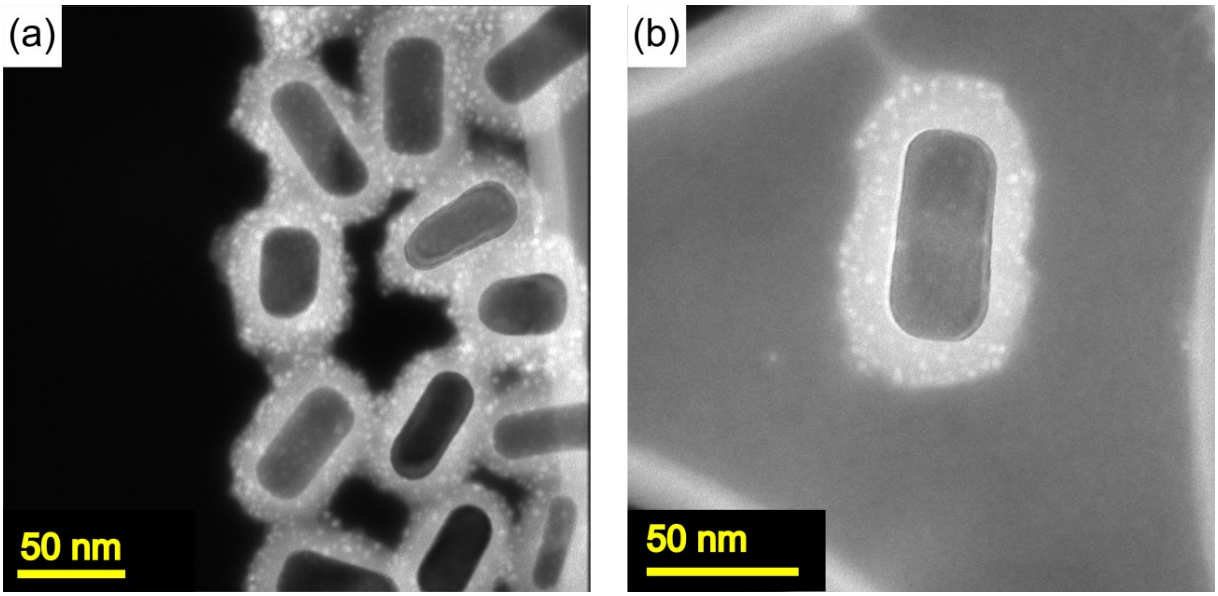

Figure S3: EFTEM images of SiNCs attached to Au@SiO2NRs prepared from AuNRs 3 with (a) 12 nm SiO2 shell, (b) 14 nm SiO2 shell.

3. Luminescence vs. dark field scattering polarization

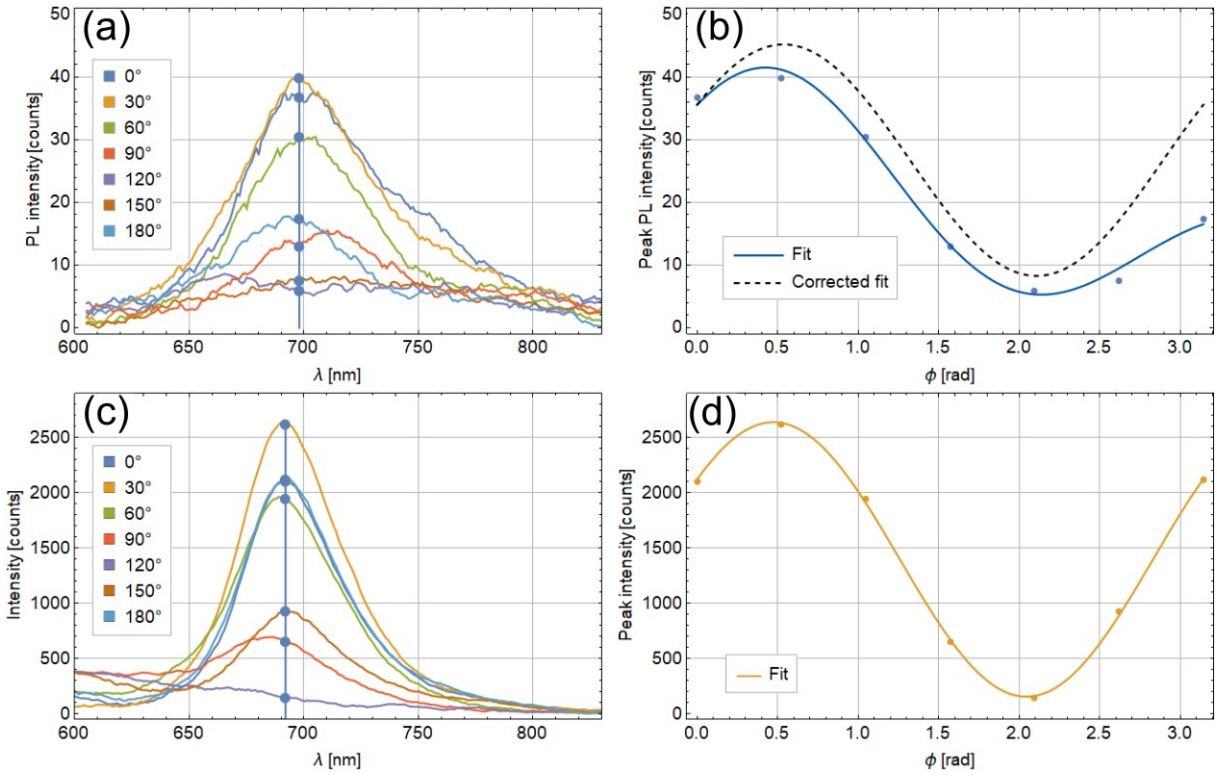

Figure S4: Single particle measurement of (a), (b) luminescence and (c), (d) dark field scattering from Au@SiO2NR@SiNCs for different polarizations. AuNRs 3 were used and the shell thickness was 12 nm. Peak values from (a) and (c) are plotted as a function of polarization in (b) and (d) respectively to visualize the same polarization dependency of PL and dark field scattering. A corrected function is shown for luminescence which accounts for gradual intensity decrease caused by long exposure of the sample to the excitation.

Figure S4 displays one practical issue of the polarization measurement – with long exposure times that had to be used due to relatively weak signal from the isolated sources, the luminescence

intensity gradually decreased during the measurement. As a result, the intensity detected at 180° (last measurement) was lower than at 0° (first measurement). The fit was therefore corrected to account for this decrease and to enable direct comparison of the polarization functions (dashed line in Figure S4).

4. Lifetime measurement

Luminescence lifetime of SiNCs attached to AuNRs with different silica shell thicknesses was measured by time gated imaging method. It is important to realize that such obtained data in fact represent an integrated intensity of the decay collected within a particular time gate rather than the luminescence decay directly. This had to be taken into account when processing the measured data as highlighted in Figure S5. The process starts with fitting the measured datapoints with such 3-exp function that its integral within the given time gate matches the corresponding datapoint value. This is shown in Figure S5b – with gate time 1µs, we are looking for a 3-exp function, whose integral from t_i to t_{i+1} (area of a column under the yellow curve) is equal to value of the datapoint at t_i (x 1µs -> area of a column under corresponding red dashed line). The fitting function thus takes the form:

$$I(t_i) = \int_{t_i}^{t_i + GW} (c_1 * e^{-\tau_1 t} + c_2 * e^{-\tau_2 t} + c_3 * e^{-\tau_3 t} + d)\, dt = \tag{1}$$

$$= \frac{c_1}{\tau_1} e^{-\tau_1 t_i} * \left(1 - e^{-GW * \tau_1}\right) + \frac{c_2}{\tau_2} e^{-\tau_2 t_i} * \left(1 - e^{-GW * \tau_2}\right) + \frac{c_3}{\tau_3} e^{-\tau_3 t} * \left(1 - e^{-GW * \tau_3}\right) + d * GW$$

where GW is the gate time width (length) and c_1, c_2, c_3, τ_1, τ_2, τ_3 and d are fit parameters. This is shown as a blue curve in Figure 4Sb for the first few datapoints and the whole integral fit is then shown in Figure 4Sa. Using the parameters of the fit we finally get the classical 3-exp function describing the luminescence intensity decay (yellow curve in Figure 4Sb):

$$I(t) = c_1 * e^{-\tau_1 t} + c_2 * e^{-\tau_1 t} + c_3 * e^{-\tau_1 t} + d \tag{2}$$

from which the mean lifetime can be extracted.

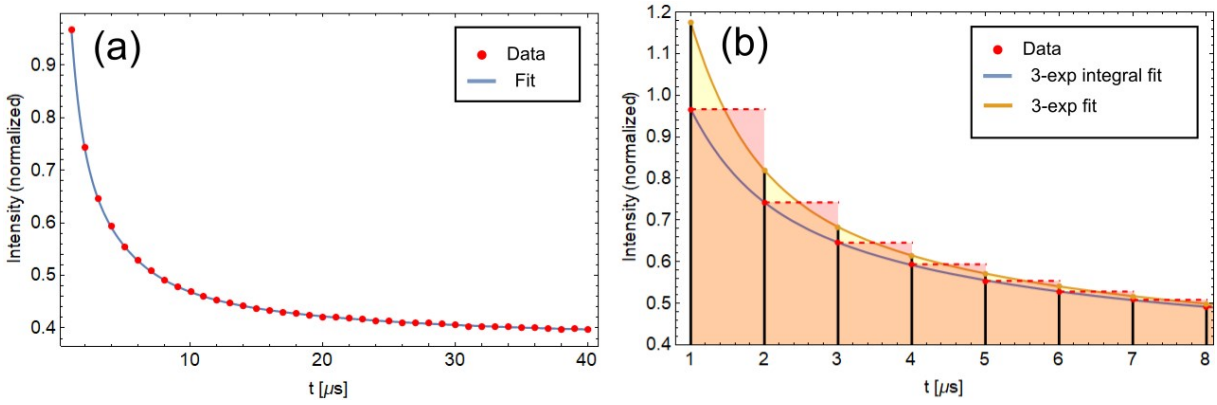

Figure S5: About fitting of the datapoints from lifetime measurements. (a) 3-exponential integral fit in the whole measurement time range. (b) 3-exponential integral fit and therefrom derived 3-exponential function describing the actual luminescence decay for the first few datapoints. The fit originates in a requirement that the integral of the 3-exponential function (yellow filling) should be equal to the integral of datapoint-based step function (red filling).

5. BEM simulations

Parameters:

The situation considered by our theoretical model is shown in Figure S6. A gold nanorod with dimensions 65.0 x 18.8 nm (length x width) is coated with a silica shell of variable thickness (2 – 20 nm). SiNCs are approximated by dipoles placed equidistantly at different positions (labelled as 1 – 20) along the nanorod's perimeter. The distance between dipoles and silica shell of 2 nm accounts for nonzero diameter of SiNCs (≈ 3.5 nm) and reduces computational time at the same time. Dielectric function of gold was taken from Johnson and Christy database[1], refractive index of porous silica was set as 1.42 and refractive index of the surrounding medium was set to 1.33 (water/ethanol/methanol). This choice of structural parameters was validated by calculating the longitudinal LSPR peak positions of Au@SiO2NRs as a function of silica shell thickness – Figure S7. In PL enhancement calculations, circularly polarized light (λ = 405 nm) travelling along the x axis is used for excitation. Emission from the dipoles was studied in a broader wavelength range of 700 – 840 nm. Radiative and nonradiative rates of the dipoles were estimated based on the measured QY and PL lifetime of SiNCs. The values were then slightly varied to obtain the best possible match with experimental PL lifetime shortening of Au@SiO2NRs@SiNCs (Figure 10c in the main text). In the end we used $\Gamma_{rad,0} = 3.4 * 10^3$ Hz and $\Gamma_{nr} = 8 * 10^4$ Hz for radiative rate and nonradiative rate, respectively. All quantities of interest (Purcell factor, excitation enhancement, total decay rate, enhancement of PL intensity) were calculated as a function of shell thickness for different positions of dipoles and for their x-, y- and z-orientations. The final shell thickness dependence was obtained by averaging results from all dipole orientations and positions.

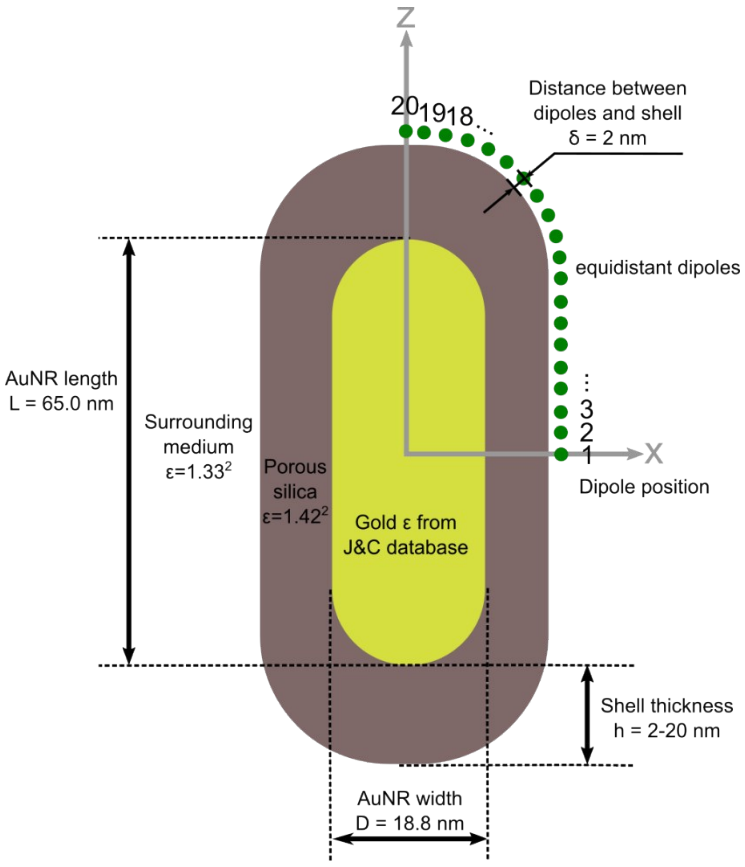

Figure S6: About the BEM model parameters, dipole positions and overall studied situation.

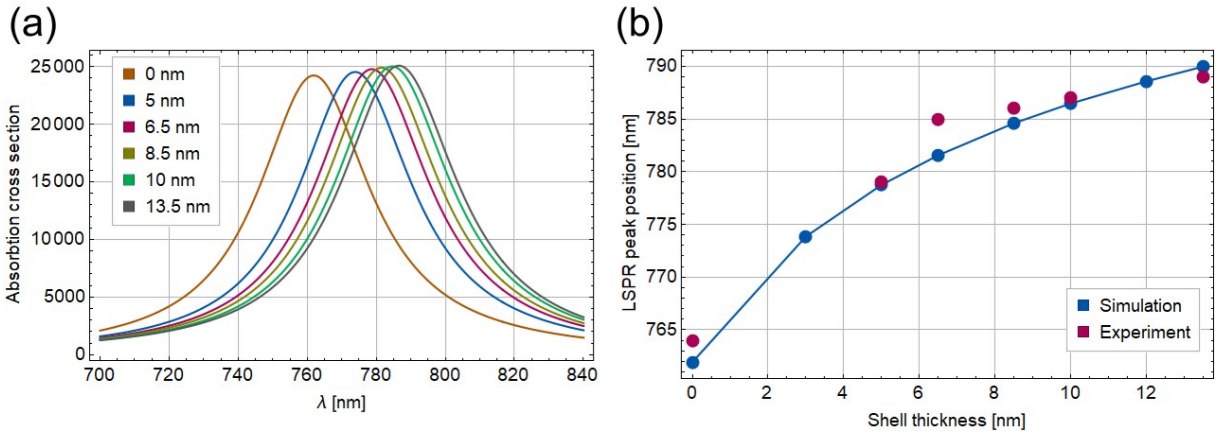

Figure S7: (a) BEM calculated longitudinal plasmonic peaks of Au@SiO2NRs with variable silica shell thickness. (b) Longitudinal LSPR peak positions as a function of the shell thickness. Values obtained from BEM simulation and experiment are compared.

When an average quantity was calculated, where partial contributions of emitters (dipoles) located at different positions to the measured PL signal are different, the result was weighted to account for the varying contributions. See for example the calculation of average total Purcell factor at the end of the next section – the mean value must be weighted by excitation intensity (I_{exc}) and far field outcoupling efficiency (represented by an external Purcell factor f_{ext}) as the emitter's contribution to the measured PL is proportional to either of these values. Furthermore, a geometrical inequality of the dipoles must be taken into consideration for averaging. The situation is explained in Figure S8. The rod-like shape of our nanoparticles naturally causes that there is much less space on the tip of the NR (dipole position 20) then on its side (dipole position 10). Therefore, assuming a homogeneous surface coverage of nanorods by SiNCs, the contribution from dipoles at different positions must be weighted by the outer surface of their respective "cylinder shells" (area between two neighboring red lines in Figure S8).

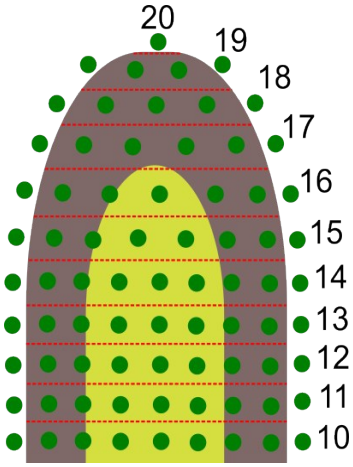

Figure S8: About geometrical factor in calculation of dipole position averaged values in BEM simulations.

Model:

In the following, a theoretical model for plasmonic enhancement of photoluminescence from a two-level system is derived. A formula for PL intensity and PL intensity enhancement under continuous excitation is shown and a model for PL decay rate enhancement under pulsed excitation is derived. The latter was used for comparison with experimental values as shown in Figure 10c.

Two-level system of nanoparticles

In a two-level system of nanoparticles, the time evolution of concentration of excited nanoparticles is described by the following differential equation:

$$\frac{dn_2}{dt} = \sigma I_{exc} n_1 - \Gamma n_2 \tag{3}$$

where n_1 and n_2 are the concentrations of non-excited and excited nanoparticles, and the total recombination (decay) rate Γ is a sum of radiative (Γ_{rad}) and non-radiative (Γ_{nr}) recombination rates. Like in refs.[2,3], by a non-radiative decay rate, we mean non-electromagnetic channels of energy dissipation. The radiative decay rate depends on particle's dielectric environment and is expressed in terms of a Purcell factor f_{tot}:

$$\Gamma = \Gamma_{rad} + \Gamma_{nr} = f_{tot}\Gamma_{rad,0} + \Gamma_{nr} \tag{4}$$

where $\Gamma_{rad.0}$ is the radiative decay rate of a nanoparticle in a homogeneous dielectric environment. The Purcell factor has its external and absorbing parts:

$$f_{tot} = f_{ext} + f_{abs} \tag{5}$$

The external part (f_{ext}) is responsible for far-field emission. The absorbing part (f_{abs}) describes electromagnetic losses in a dielectric environment of a nanoparticle such as quenching and absorption. The photoluminescence intensity I_{PL} is given by:

$$I_{PL} = \alpha n_2 f_{ext} \Gamma_{rad,0} \tag{6}$$

where α is a proportionality factor.

PL intensity enhancement under constant excitation

In a steady state, dn_2/dt = 0 and

$$n_2 = \frac{\sigma I_{exc} n}{\sigma I_{exc} + \Gamma_{rad} + \Gamma_{nr}} \tag{7}$$

where $n = n_1 + n_2$ = const. is the total concentration of nanoparticles. Using (4) and (5) we get for the PL intensity:

$$I_{PL} = \frac{\alpha\sigma n I_{exc} f_{ext} \Gamma_{rad,0}}{\sigma I_{exc} + \Gamma_{nr} + f_{tot}\Gamma_{rad,0}} \tag{8}$$

In case of a weak excitation ($\sigma I_{exc} \ll \Gamma$) we can write:

$$I_{PL} = \alpha\sigma n I_{exc} \frac{f_{ext}\Gamma_{rad,0}}{\Gamma_{nr} + f_{tot}\Gamma_{rad,0}} \tag{9}$$

The corresponding PL enhancement factor for dipoles near Au nanorods compared to dipoles in homogeneous dielectric environment is:

$$\xi = \frac{I_{PL}}{I_{PL,0}} = \frac{I_{exc}}{I_{exc,0}} * \frac{f_{ext}(\Gamma_{nr} + \Gamma_{rad,0})}{\Gamma_{nr} + f_{tot}\Gamma_{rad,0}} = \xi_{exc} * \xi_{QY} \tag{10}$$

where ξ_{exc} is the excitation enhancement and ξ_{QY} is the quantum yield enhancement. In the above formula ξ_{exc} has to be averaged over excitation directions and excitation polarizations, f_{ext} and f_{tot} have to be averaged over orientations of electric dipoles which approximate the emission of SiNCs.

PL decay rate enhancement under pulsed excitation

Under pulsed excitation, the time evolution of PL from NCs located at the i-th position is set by equation (6) and has the form:

$$I_{PL}^{(i)}(t) = \alpha f_{ext}^{(i)} \Gamma_{rad,0} \times n_{2,0}^{(i)} e^{-\Gamma^{(i)} t} \tag{11}$$

The initial concentration of excited NCs at the i-th position ($n_{2,0}^{(i)}$) is proportional to the excitation intensity at this position and thus:

$$I_{PL}^{(i)}(t) = \alpha\beta I_{exc}^{(i)} f_{ext}^{(i)} \Gamma_{rad,0} e^{-\Gamma^{(i)} t} \tag{12}$$

where β is the proportionality factor. The average decay rate can be found as the weighted arithmetic mean. Note that the weight of a relative surface area $S^{(i)}$ has to be also considered here, as described in Figure S8:

$$\Gamma^{ave} = \frac{\sum_i I_{exc}^{(i)} f_{ext}^{(i)} S^{(i)} \Gamma^{(i)}}{\sum_i I_{exc}^{(i)} f_{ext}^{(i)} S^{(i)}} = \Gamma_{nr} + \Gamma_{rad.0} \cdot f_{tot}^{ave} \tag{13}$$

where f_{tot}^{ave} is the average Purcell factor:

$$f_{tot}^{ave} = \frac{\sum_i I_{exc}^{(i)} f_{ext}^{(i)} S^{(i)} f_{tot}^{(i)}}{\sum_i I_{exc}^{(i)} f_{ext}^{(i)} S^{(i)}} \tag{14}$$

and $f_{tot}^{(i)}$ is the total Purcell factor of a dipole located at the i-th position.

Complementary BEM simulation results:

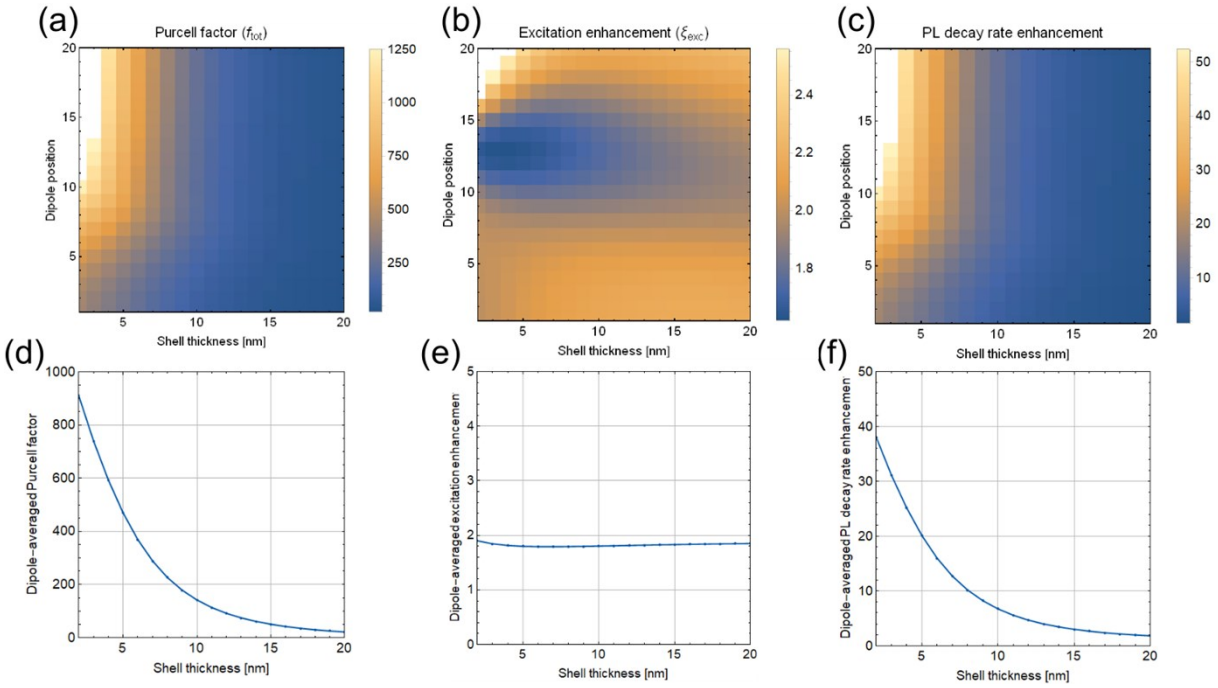

Figure S9: Complementary BEM simulation results for (a,d) Total Purcell factor, (b, e) Excitation enhancement and (c,f) PL decay rate enhancement. In (a, b, c) the results are displayed for individual dipoles placed at different locations with different silica shell thickness, in (d, e, f) dipole position averaged results are shown. In all panels the results are averaged over the dipole orientations.

References:

[1] P. B. Johnson, R. W. Christy, *Phys. Rev. B* 1972, *6*, 4370.

[2] G. W. Ford, W. H. Weber, *Phys. Rep.* 1984, *113*, 195.

[3] J. Valenta, M. Greben, S. A. Dyakov, N. A. Gippius, D. Hiller, S. Gutsch, M. Zacharias, *Sci. Rep.* 2019, *9*, 11214.